Chemical Science

RSC Publishing

EDGE ARTICLE

View Article Online
View Journal | View Issue

Cite this: *Chem. Sci.*, 2013, **4**, 677

Tunneling control of chemical reactions: C–H insertion *versus* H-tunneling in *tert*-butylhydroxycarbene†

David Ley, Dennis Gerbig and Peter R. Schreiner*

Received 19th September 2012
Accepted 25th October 2012

DOI: 10.1039/c2sc21555a

www.rsc.org/chemicalscience

Elusive *tert*-butylhydroxycarbene was generated in the gas phase *via* high-vacuum flash pyrolysis of *tert*-butylglyoxylic acid at 960 °C. The pyrolysis products were subsequently matrix isolated in solid Ar at 11 K and characterized by means of IR spectroscopy. While still being exposed to the harsh pyrolysis conditions, the hydroxycarbene undergoes CH-insertion to dimethylcyclopropanol, as well as a CC-insertion to novel methylbutenol, with activation barriers of 23.8 and 31.0 kcal mol^{-1}, respectively. Once embedded in the cold Ar matrix, the carbene transforms to its isomer pivaldehyde not only by photolysis, but it also cuts through the barrier of 27.3 kcal mol^{-1} by quantum mechanical tunneling. The temperature independent half-life is measured as 1.7 h; the tunneling pathway was entirely blocked upon *O*-deuteration. The experimental half-life of *tert*-butylhydroxycarbene was verified by tunneling computations applying the Wentzel–Kramers–Brillouin formalism on the minimum energy path evaluated at the computationally feasible M06-2X/6-311++G(d,p) level of theory. Our experimental findings are supported by relative energy computations at the CCSD(T)/cc-pVDZ level of theory.

Introduction

Tunneling, the ability to overcome potential energy barriers despite of a lack of energy to surmount them,[1,2] is a theoretically reasonably well understood yet unappreciated phenomenon in chemistry.[3] While quantum mechanical tunneling (QMT) is often considered merely a correction to the rate of a reaction[4–10] we have demonstrated recently that it must be considered as the third form of chemical reaction control next to thermodynamic and kinetic control.[11] Here we describe the preparation of a new molecular system where *tunneling control*[3,12,13] ensues in the sense that the formally more stable product forms although it is associated with a higher barrier.[14] This supports and generalizes our findings for methylhydroxycarbene (**1**) that undergoes facile [1,2]H-tunneling to give the thermodynamic product acetaldehyde (**2**), although the barrier for formation of vinyl alcohol (**3**) is considerably lower (by about 5 kcal mol^{-1}).[12] This situation can be rationalized with the notion that barrier width (which has a linear relationship to the barrier penetration integral) trumps barrier height (which correlates with its square root).[15] We have recently shown that the novel family of hydroxycarbenes (R–C–OH) is ideally suited to study these phenomena as they break[3] the classic rules[11,16,17] of kinetic *vs.* thermodynamic control by means of QMT.[15,18–21] They nicely complement and expand the well-established reactivity patterns of many other donor-substituted carbenes.[22–29]

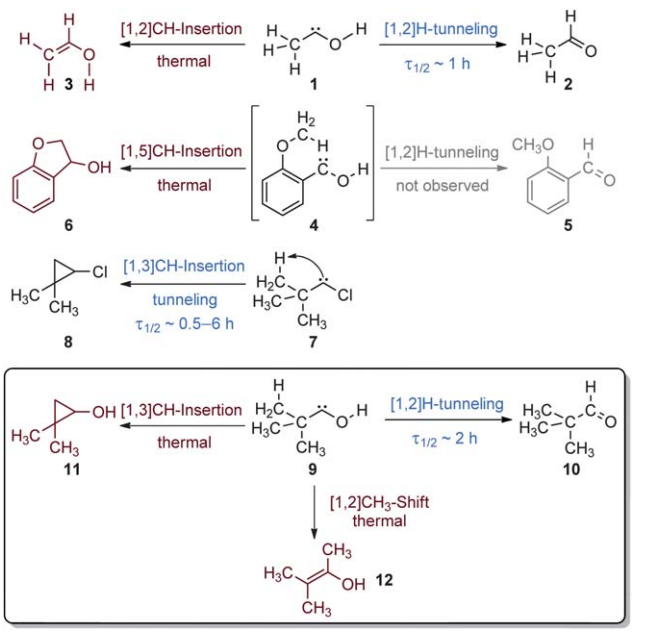

Scheme 1 Competing pathways of [1,2]H-tunneling shifts *vs.* [1,*n*]CH-insertions in hydroxycarbenes **1**, **4**, and **9** as well as *tert*-butylchlorocarbene (**7**).

Institute of Organic Chemistry, Justus-Liebig University, Heinrich-Buff-Ring 58, Giessen, Germany. E-mail: prs@org.chemie.uni-giessen.de; Fax: +49 641-9934309; Tel: +49 641-9934300

† Electronic supplementary information (ESI) available: Full matrix IR spectra of the pyrolyses of **13** and *d*-**13** and reference spectra of **2**, **10**, **11**, **13**, **14**, and **16**; synthesis of **11**; optimized geometries, energies, and ZPVEs of all computed species; crystallographic data; full references for computational chemistry codes; kinetic plots showing the decay of **9**. CCDC reference number 900416. For ESI and crystallographic data in CIF or other electronic format see DOI: 10.1039/c2sc21555a

For instance, matrix-isolated *tert*-butylchlorocarbene (**7**, Scheme 1) undergoes a [1,3]CH-insertion reaction to **8** by a tunneling mechanism within 0.5–6 h at 11 K.[30] Similarly, phenylhydroxycarbene exclusively gives benzaldehyde through facile H-tunneling within 2.5 h.[31]

As neither carbene is an ideal substrate to examine competing reaction paths as for **1**, we had initially hoped that *o*-methoxyphenylhydroxycarbene (**4**) would provide evidence for both the intramolecular CH-insertion of the intermediate hydroxycarbene and a competing [1,2]H-shift driven by tunneling. However, **4** cannot be observed directly and only the insertion product was detected.[32] Hitherto unknown *tert*-butylhydroxycarbene (**9**) appeared to be an ideal system to provide another firm example for tunneling control as there are several competing reaction paths with largely different kinetic barriers and thermodynamic driving forces (Scheme 1). As **7** undergoes a tunneling [1,3]CH bond insertion, we were particularly interested in determining if that is also the case for **9**, leading to cyclopropyl alcohol **11**, or if the expected [1,2]H-tunneling shift to **10** is indeed faster despite a higher barrier, which is, however, expected to be narrower. We also consider the [1,2]CH_3-shift of **9** to enol **12** as a viable reaction path for yet another competing process with a barrier that is predicted to be both high and wide and thus not susceptible to tunneling.

Our recent work on the preparation and identification of several hydroxycarbenes[12,31,33] revealed a dependency of the H-tunneling half-lives on the electronic properties of the carbene substituents: stronger electron donors entail longer half-lives for the H-tunneling process, culminating in the supression of H-tunneling for hydroxycarbenes with a second heteroatom on the carbene carbon.[27,29] In the course of our ongoing work on hydroxycarbenes we were able to show that the intrinsic reactivity that comes along with the low-valent carbon not only drives the [1,2]H-shift, but as well rapidly occurring thermal reactions that are characteristic for carbenes: both **1** and **4** undergo CH-insertion,[12,32] while cyclopropylhydroxycarbene also displays an intramolecular CC-insertion.[13] With the [1,2]H-shift to the corresponding aldehyde being the only known tunneling reaction in hydroxycarbenes to date, the question arises whether **9** behaves likewise, or if it is more akin to its other parental side (Scheme 1), *i.e.*, **7**, which is an example for heavy atom tunneling through a barrier of 7 kcal mol^{-1}.[30] We were curious if **9** could possibly represent a system with two competing tunneling pathways, namely light and heavy atom tunneling in the same molecule: the kinetics of the [1,2]H-tunneling mechanism ascribed to the hydroxycarbene side was expected to parallel that of structurally related **1**. Assuming that the hydroxyl group has similar electronic effects on the barrier width as the chlorine substituent in **7**, we initially supposed that **9** would have two tunneling pathways that were roughly equal in terms of tunneling rates: light-atom tunneling through the barrier of the [1,2]H-shift and heavy-atom tunneling through that of the [1,3]CH-insertion.

Results and discussion

Pyrolysis of the precursor

All energies in this paragraph were evaluated by computing relative CCSD(T)/cc-pVTZ single point energies for structures optimized at the M06-2X/6-311++G(d,p) level of theory, employing the latter one's zero point vibrational energy (ZPVE). We chose the underlying level of theory for structural computations, because it has shown to provide accurate computational data for hydroxycarbenes.[13,32,34] According to the computational results (Scheme 2), the only passable reaction for the carbene precursor **13** is CO_2 extrusion over a barrier of 38.4 kcal mol^{-1} (**TS1**) yielding the desired hydroxycarbene **9**. A four-membered transition state (**TS2**) for decarboxylation directly leading to **10** can be located computationally, but is insignificant due to the sizeable activation barrier of 73.2 kcal mol^{-1}; similarly, the concerted extrusion of isobutylene from **13** over **TS3** has no practical relevance owing to an even higher activation barrier of 86.3 kcal mol^{-1}.

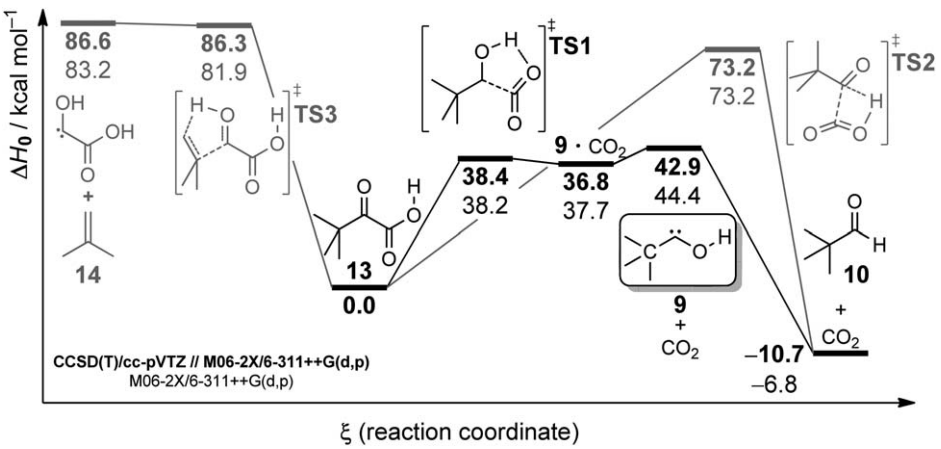

Scheme 2 Potential energy hypersurface of *tert*-butylglyoxylic acid (**13**): decarboxylation to the hydroxycarbene **9** and rearrangement to the products **10** + CO_2 are the only thermally accessible reactions under our conditions. The carbene forms a weakly bound CO_2 complex, which can be located computationally but is not persistent under the pyrolysis conditions due to rapid dissociation into the carbene and CO_2.

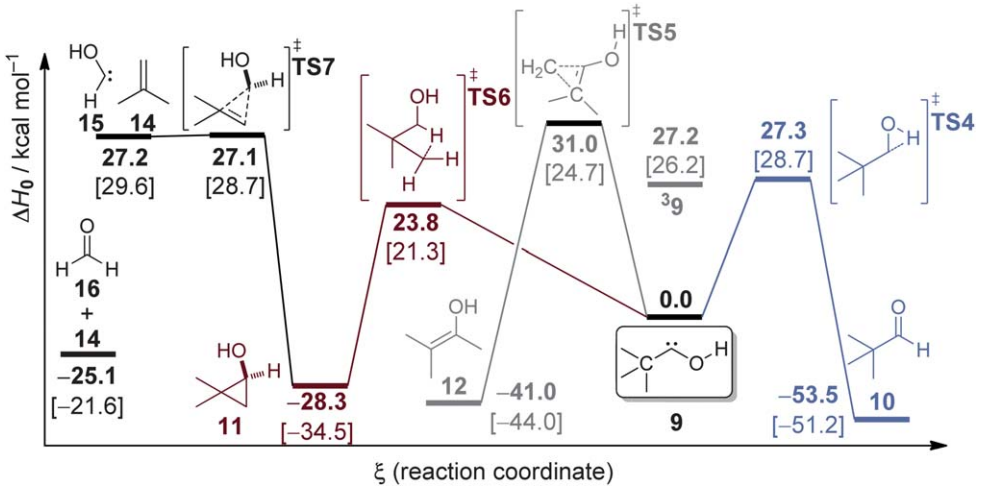

Scheme 3 ZPVE-corrected PES around **9**; bold type face: CCSD(T)/cc-pVDZ; in brackets: M06-2X/6-311++G(d,p). The hydroxycarbene features three pathways with different activation barriers. While **11** and **12** form concomitantly with the carbene during pyrolysis, the reaction towards **10**, thus the one with the highest activation barrier, still occurs in the kinetically stabilizing matrix *via* QMT.

As high-vacuum flash pyrolysis (HVFP) is a non-equilibrium process and we cannot evaluate the contact time of the molecules in the pyrolysis zone, it is impossible to establish a link between the temperature of the pyrolysis zone and the upper limit of thermally accessible reaction paths. We were able to roughly estimate this limit by experimental means: while methyl bromide remains unchanged under the applied HVFP conditions (960 °C), methyl iodide undergoes cleavage of the C–I bond. With the bond dissociation energies for the two halomethanes[35] being 69.8 and 56.1 kcal mol^{-1}, respectively, the upper limit of energetic accessibility must be in between the two values, *i.e.*, around 60 kcal mol^{-1}. We can exclude radical cleavage of **13**, as we had no spectroscopic evidence for the *tert*-butyl radical in the pyrolysis mixture,[36] and as comparative considerations based on related systems[37] indicate a dissociation energy of almost 80 kcal mol^{-1} that is far above the possible limit of our pyrolysis apparatus. Surprisingly, the pyrolysis mixture of **13** does not only contain **9**, but a variety of other compounds (namely **10–12**, **14**, **16** and **17**). This must be due to consecutive reactions of **9**.

Reactions in the pyrolysis zone

Paralleling the reactivity of other *tert*-butyl carbenes, the reaction path with the lowest activation barrier (**TS6**; 23.8 kcal mol^{-1}) for **9** leads to the cyclic insertion product **11**, which is the kinetic product that should preferentially form as long as there is enough energy in the system to overcome this barrier—a condition that can be assumed for molecules passing the pyrolysis zone.[38]

The [1,2]H-shift over the sizable barrier of 27.3 kcal mol^{-1} (**TS4**) would give the thermodynamic product **10** and a third, energetically intermediate reaction path, yields 2,3-dimethylbuten-2-ol (**12**) *via* a shift of a methyl group (**TS5**). Whereas **10**, **11** as well as the keto-isomer of **12** (*i.e.*, **17**) could easily be identified by comparison with the IR spectra of the pure matrix isolated compounds (either commercially available, or synthesized as in the case of **11**; see ESI†), some IR absorptions of **12** were assigned by comparison with the computed vibrational frequencies. While **10** and **12** were only present in rather small amounts, the abundance of **11** as well as of its degradation products indicate that the reaction pathway with the lowest activation barrier is favoured within the pyrolysis zone.

Dimethylcyclopropanol (**11**), the insertion product of **9**, undergoes degradation reactions in the pyrolysis zone (Scheme 4). Aldehyde **10** can be detected in the pyrolysis mixture of **11** (also prepared independently), so that the reverse process of the hydroxycarbene's CH-insertion must occur. The abundance of isobutylene (**14**) and formaldehyde (**16**) in the pyrolysis mixture of **11** provides evidence for another degradation process, namely retro-cyclopropanation (through **TS7**, Scheme 3). Intermediate hydroxycarbene **15** must carry enough excess energy to allow rapid isomerization to the respective aldehyde prior to matrix isolation, thereby avoiding direct spectroscopic identification.

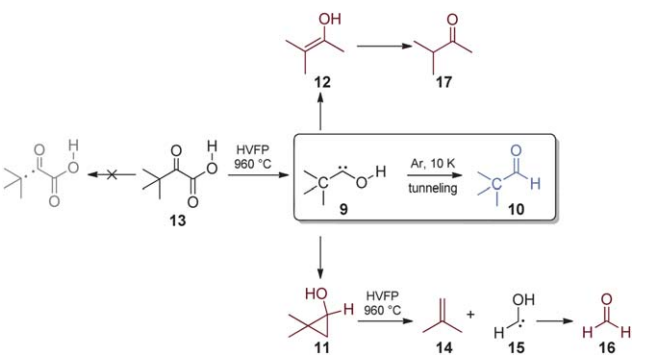

Scheme 4 Thermal decarboxylation of *tert*-butylglyoxylic acid (**13**) yields the desired *tert*-butylhydroxycarbene **9**, which undergoes subsequent thermal (red) as well as tunneling (blue) reactions. There is no experimental evidence for radical cleavage (grey) of **13**.

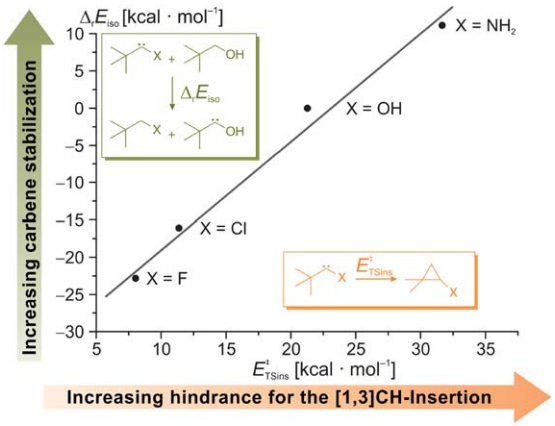

Scheme 5 Correlation between the isodesmic reaction energy as a measure of substituent stabilization in *tert*-butyl carbenes and the activation barrier for the respective insertion at M06-2X/6-311++G(d,p).

Carbene preparation and identification

Tert-butylhydroxycarbene **9** was prepared by thermal gas-phase decarboxylation of *tert*-butylglyoxylic acid (**13**, Scheme 4), which was synthesized through SeO_2 oxidation of commercially available *tert*-butyl methyl ketone. The precursor (**13**) was allowed to slowly evaporate into the pyrolysis zone of our matrix apparatus (see Experimental section for details). The pyrolyses were typically carried out at a temperature of 960 °C, the highest accessible temperature for our experimental setup. In contrast to other hydroxycarbenes, the IR spectra of the pyrolyses mixtures of **13** showed rather small amounts of the carbene itself, but dimethylcyclopropanol (**11**)—the [1,3]CH bond insertion product of **9** (*vide supra*)—was clearly observable, as was the aldehyde (**10**). We also found traces of **12**, which is the [1,2]CH_3-shift product of **9**. Both isobutylene (**14**) and formaldehyde (**16**) were present in the pyrolyses mixtures, indicating further degradation of **9** or one of its reaction products.

The UV absorption maximum of **9**, computed with time-dependent perturbation theory (TD-MP2) at the MP2/cc-pVTZ level, was determined as $\lambda_{max} = 361$ nm ($^1A' \rightarrow {}^1A''$, open shell) and short exposure of the matrix to 366 nm light from a high-pressure mercury lamp led to complete disappearance of the carbenes IR bands, in favour of rising IR bands of **10**.

This photo-induced transformation of **9** to **10** allowed matching the carbene's IR absorptions (ν) with the CCSD(T)/cc-pVDZ computed harmonic vibrational frequencies (ω) of the energetically favourable conformation of **9** with the OH group pointing away from the *tert*-butyl group and an *s-trans*-conformation of the HOCC moiety (Fig. 1 and Table 1).

The agreement between the experimental and scaled (by a factor of 0.9788) (ref. 39) harmonic vibrational frequencies is generally very good (Table 1), with the largest deviation of 4% for the highly anharmonic OH stretch. This noticeable

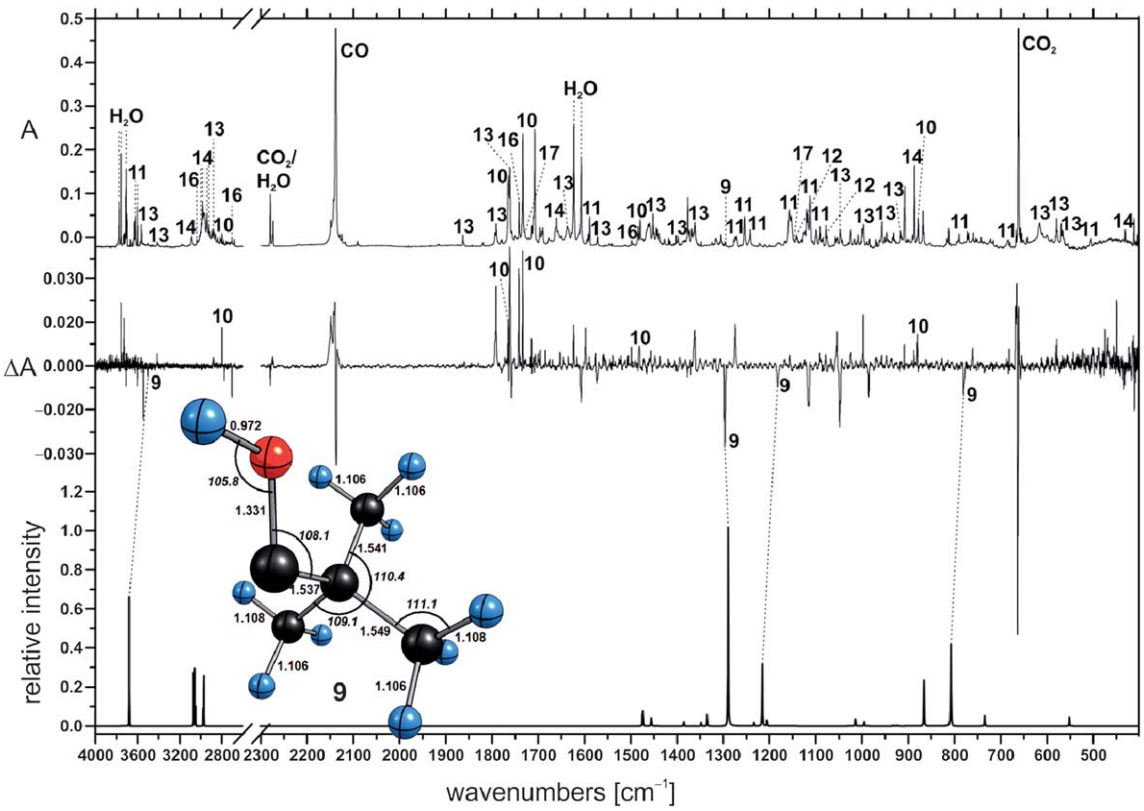

Fig. 1 IR spectrum of pyrolysis mixture of **13** (top) and corresponding difference spectrum after 5 min of irradiation at 366 nm (middle); disappearing signals point downward and are matched with the computed spectrum of **9** (bottom) [CCSD(T)/cc-pVDZ, frequencies scaled with a factor of 0.9788]. Difference bands are due to the formation of **10**, as well as interconversion of two isomers of **13**. The pyrolysis was carried out at 960 °C.

Table 1 Experimental (ν) and computed harmonic vibrational frequencies ω (unscaled) and ω' (scaled with a factor of 0.9788)(in cm^{-1}) of **9** (C_1) and *d*-**9** [CCSD(T)/cc-pVDZ]; I_{theor} in km mol^{-1}

Approx. description	ν	I_{obs}	ω	ω'	I_{theor}
*$(H_3C)_3C$–OH (**9**)*					
OH str.	3546	w	3755	3675	104
	3544				
CO str.	1297	s	1317	1289	154
	1296				
COH def.	1183	w	1242	1216	46
OH o.o.p. def.	780	s	825	808	79
*$(H_3C)_3C$–OD (*d*-**9**)*					
CH str.	3062	w	3132	3066	39
CH str.	3049	w	3119	3053	47
OD str.	2662	m	2735	2677	59
	2660				
CO str.	1291	s	1324	1296	109
	1290				
COD def.	607	w	639	625	46

difference also appears in the relative deuterium shifts (experimental: 884 cm^{-1}; computational: 998 cm^{-1}). This common observation for hydroxycarbenes for the OH and OD stretching vibrations is due to their strongly anharmonic character. The minimum energy conformation of **9** at the CCSD(T)/cc-pVDZ level of theory is C_S symmetric (Fig. 1), but has a very small imaginary vibrational mode ($7i$ cm^{-1}).

H-tunneling in *tert*-butylhydroxycarbene (9)

The reaction barriers surrounding **9** are too high to be overcome at the temperatures of our noble gas matrices, as 11 K would only allow a process to take place with an activation barrier at the very most of 2 kcal mol^{-1}. Similar to other hydroxycarbenes, the IR bands of **9** vanish following first-order kinetics with a half-life of 1.7 h in favour of the bands of **10**. During the rate determination the matrix was carefully shielded from external light so that photochemical reactions can be excluded. While the tunneling half-life of the closely related methylhydroxycarbene[12] shows strong sensitivity to the matrix material, we did not measure much of an effect for **9**, as varying the matrix material (Ar, Kr and Xe) only affects the tunneling half-lives slightly beyond our error tolerance, with a trend toward longer tunneling half-lives in the heavier noble gases (2.2 h in Kr, 2.8 h in Xe).

Our computations support the experimental evidence of QMT accounting for the decay of **9**: using the Wentzel–Kramers–Brillouin (WKB)[40] formalism, which gave good results for our previously reported hydroxycarbenes,[12,13,31–33] we computed the [1,2]H-tunneling half-life of **9** as 0.4 h, in good agreement with the experimental value of 1.7 h. The computed half-life of the *O*-deuterated species is in the range of 10^3 years, in accordance with our experiments that did not indicate its decay (over a time period of at least several days). The other two reactions, namely the insertion of **9** to **11**, as well as the [1,2]CH_3-shift from **9** to **12** both show negligible QMT contributions resulting in computed half-lives of 10^{31} and 10^{40} years, respectively.

The system thus provides another example of *tunneling control*, since the reaction through the higher, but narrower [1,2] H-shift barrier is feasible at cryogenic conditions whereas the higher masses that are involved in the CH-insertion and the CH_3-shift entail much broader barriers through which tunneling is unlikely. The related system *tert*-butylchlorocarbene (**7**) does feature QMT through the CH-insertion barrier, since it only amounts to 8.0 kcal mol^{-1}, compared to the 23.8 kcal mol^{-1} for **9**. Strong electron donors entail higher barriers for the [1,3]CH-insertion process as they stabilize the carbene. This can be probed by evaluating the isodesmic equation for formal H_2 transfer with *tert*-butanol. The endothermicity of this hypothetical reaction inversely correlates with carbene stability, which in return entails higher barriers for the [1,3]CH-insertion.

Comparison of barrier shapes

As outlined above, **9** undergoes three different unimolecular reactions (Scheme 4) in the diluted gas phase of the pyrolysis zone: estimates of the pyrolysis product distribution show that a major portion of the carbene undergoes CH-insertion, while a smaller part overcomes the barrier to the aldehyde, either thermally or by thermally activated tunneling,[18,41–43] and an even smaller portion undergoes [1,2]CH_3-shift to **12**. The product distribution is in accordance with classic kinetic and thermodynamic control of the reaction: for reactions in the pyrolysis zone, one can have kinetic or thermodynamic control, where the decisive factor is the amount of energy that the carbene receives from collisions with the hot wall. While the formation of **11** is favoured for particles with less energy due to the lowest possible activation barrier, particles that bear more thermal energy will underlie thermodynamic control and thus favour the reaction to **10**. The barrier for the CH_3-shift reaction of **9** to **12** is too high to allow kinetic control, but too broad to allow tunneling control. With the reaction energy being too small for thermodynamic control, it is obvious that this reaction is strongly disfavoured, thereby explaining why the product of this path is scarcely formed.

In the cold matrix, *tunneling control* prevails, which is evident from the experimentally observable decay of **9** to **10**. As also found for carbene **4**,[32] we have no evidence for a tunneling contribution to the CH-insertion in **9** which only forms in the pyrolysis zone. In contrast, while the activation barrier for the isomerization of **7** to **8** has the same width it still allows tunneling due to its much smaller height (Fig. 2). Our spectroscopic investigations reveal that the decay of **9** (see ESI for evaluation of the half-lives†) corresponds to an increase of **10**, while at the same time the concentrations of **11** and **12** remain unchanged. It is thus evident that [1,2]H-tunneling dominates the low temperature reactivity of **9**, thereby paralleling the reactivity of some previously reported hydroxycarbenes. In order to qualitatively compare the three reaction pathways, we evaluated the minimum energy path for each system and each direction at the M06-2X/6-311++G(d,p) level of theory, augmented with CCSD(T)/cc-pVDZ single point energies (Fig. 2). It is obvious that the activation barriers for the [1,2]H-shift in the two hydroxycarbenes **4** and **9** are very small and thereby allow barrier penetration, while the insertion barrier in the

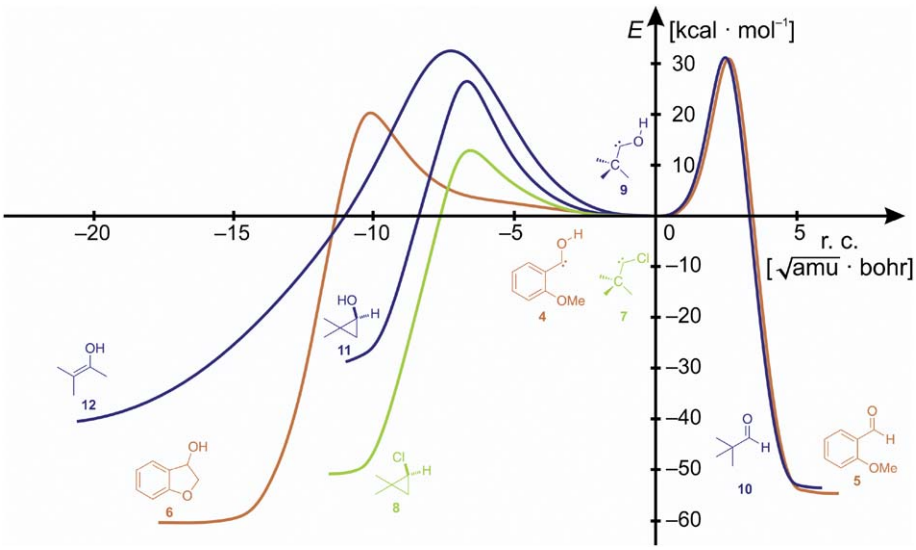

Fig. 2 Comparison of the competitive minimum energy paths [CCSD(T)/cc-pVDZ//M06-2X/6-311++G(d,p)] of several carbenes. The reaction profiles of **9** to **11** and **12** (blue) are too broad and too high to allow QMT.

chlorocarbene **7** is broader and only susceptible to tunneling due to its much smaller height. Structures **4** and **9** are conceptually different in their energy profiles of possible products: the PES of **9** represents a generic example for a system featuring the possibility of kinetic, thermodynamic, and tunneling control. We could experimentally observe all products, since we were able to matrix-isolate a complex mixture from the pyrolysis zone. In contrast, the thermodynamic product of **4** is also the one with the lower barrier so that both kinetic and thermodynamic control favor its formation, and accordingly, we could neither detect **4** nor its respective aldehyde **5** experimentally.

Conclusion and outlook

In the prevalent notion of kinetic *vs.* thermodynamic control, the decisive factor for the outcome of a chemical reaction with several accessible pathways is based on the differences in the activation barriers. This concept has been challenged by the experimental observation that many matrix isolated hydroxycarbenes isomerize in the direction of the higher barrier, while the reaction over (or through) the lower barrier does not take place. We introduced the term *tunneling control*, reflecting that chemical selectivity is not only determined by relative barrier heights, but also barrier widths. The reaction coordinate is a crucial property of a chemical reaction that needs to be treated carefully in order to allow the qualitative estimation of QMT contribution, and thus to fully understand and evaluate chemical selectivity.

The classic rule of thermodynamic *vs.* kinetic control is not the only established concept that is violated by the behavior of carbene **9**, as also is the Hammond-postulate,[44] an intuitive rule that links the energetic profile of a reaction with the position of the TS: its relative position on the reaction coordinate is supposed to be closer to the reactant, the more exergonic a reaction is. Comparing the [1,3]CH-insertion and the [1,2]CH_3-shift in **9**, one can see that this rule is inverted here, since the earlier TS leads to the energetically less stable product **11**.

Experimental section

Precursor preparation

To a solution of 2 g (20 mmol) commercially available 3,3-dimethyl-2-butanone (pinacolone) in 8 mL dry pyridine were slowly added 3.33 g (30 mmol) of SeO_2 and the reaction mixture was heated to 130 °C for 90 min. After filtration, concentration of the reaction mixture gave a brown oil that was dissolved in 20 mL of 5% sodium hydroxide solution and washed three times, each with 20 mL diethyl ether. The aqueous layer was acidified with diluted HCl and extracted three times with 20 mL methylene chloride. The organic layer was dried over sodium sulfate and distilled *in vacuo*; yield: 1.06 g *tert*-butylglyoxylic acid (41%); b.p. 62 °C at 35 mbar. ^{1}H-NMR ($CDCl_3$): $\delta = 1.24$ (s, 3 CH_3); $\delta = 10.54$ (s, OH). ^{13}C-NMR (400 MHz, $CDCl_3$): $\delta = 25.65$ ($(H_3C)_3$–C–C(O)–COOH); $\delta = 42.6$ ($(H_3C)_3$–*C*–C(O)–COOH); $\delta = 164.6$ ($(H_3C)_3$–C(O)–*C*OOH; $\delta = 201.1$ ($(H_3C)_3$–*C*(O)–COOH). The colorless liquid slowly forms a crystalline dimer if stored at 5 °C. The structure of the dimer, which we found by means of X-ray crystal structure determination (Fig. 3, for details see ESI†) is in accordance with the suggestion made by Schellenberger and Oehme[45] in 1964. The dimer transforms into its monomer by distillation, or in the course of 2–3 weeks if stored above 20 °C.

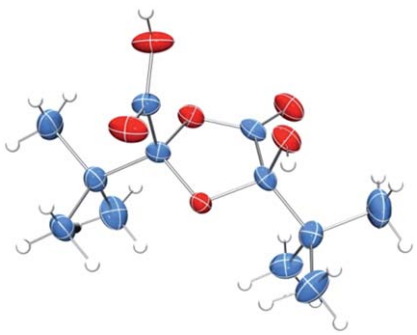

Fig. 3 Crystal structure ($P2_1/c$) of the dimer of **13** (50% probability ellipsoids).

Matrix isolation experiments

For the matrix isolation studies, we used an APD Cryogenics HC-2 cryostat with closed-cycle refrigerator system, equipped with an inner CsI window allowing IR measurements. Spectra were recorded with a Bruker IFS 55 FT-IR spectrometer with a spectral range of 4500–300 cm^{-1} and a resolution of 0.7 cm^{-1}. For the combination of high-vacuum flash pyrolysis with matrix isolation, we employed a small, custom built water-cooled oven based on a quartz tube of 80 mm length and 8 mm diameter, which was directly connected to the vacuum shroud of the cryostat. The quartz tube could be resistively heated by a coaxial wire and thus served as the pyrolysis zone and its temperature was monitored by means of a NiCr–Ni thermocouple. *Tert*-butylglyoxylic acid and dimethylcyclopropanol were evaporated at −35 °C from a storage bulb into the quartz pyrolysis tube. At a distance of approximately 50 mm, all pyrolysis products were mixed with a large excess of Ar (typically 60–120 mbar from a 2000 mL storage bulb) and condensed on the surface of the cold (11 K) matrix window. A high-pressure mercury lamp (Osram HBO 200) in combination with a monochromator (Bausch & Lomb) was used as a light source for irradiation.

Computational methods

The PES of **9** was computed utilizing the CFOUR[46] program package for coupled-cluster single and double excitations (with perturbatively included triple excitations) [CCSD(T)],[47–50] using the frozen core approximation and the Dunning-type correlation consistent basis set cc-pVDZ,[51] as well as analytically computed vibrational harmonic frequencies. We used this level of theory as a benchmark to measure the results of computationally less expensive methods: while MP2/cc-pVTZ fails to describe the PES of **9**, our SCS-MP2 results using ORCA[52–54] were much closer to the CCSD(T) benchmark, yet the relative barrier heights could still not be reproduced. Considering the barrier for the [1,2]H-shift, the results of our M06-2X/6-311++G(d,p)[55,56] computations performed with Gaussian09 were in excellent agreement with the CCSD(T)/cc-pVDZ benchmark. This is in accordance with our observation on previously reported hydroxycarbenes, wherein this level of theory gave good results for computed tunneling half-lives. Admittedly, the rather strong deviation between the M06-2X and the CCSD(T) energy considering the barrier of the CH_3-shift (Scheme 3) tells us that the results of this functional have to be handled with care. At the same time, the close agreement of the two methods considering the [1,2]H-shift tunneling reaction in **9** justifies the usage of the M06-2X functional in describing this particular reaction and thus justifies computationally feasible tunneling half-lives based on the WKB approximation at this level of theory: for each examined reaction, we computed the intrinsic reaction path (IRP) and the zero-point vibrational energy corrections (ZPVE) of the projected frequencies along the path at the M06-2X/6-311++G(d,p) level of theory utilizing the Hessian-based predictor corrector algorithm,[57] as implemented in Gaussian09.[58] Tunneling probabilities were evaluated by computing one-dimensional barrier penetration integrals along the IRP and invoking the WKB relation.[40] By setting the attempt energy of the particle equal to the zero-point energy of the frequency that corresponds to the reaction coordinate, tunneling half-lives could be evaluated from the tunneling probabilities. Algebraic equations were solved with the Mathematica program package.[59]

Acknowledgements

We gratefully acknowledge funding by the Deutsche Forschungsgemeinschaft, ERA-Chemistry and the Fonds der Chemischen Industrie. We thank Wesley D. Allen and Attila G. Császár for stimulating discussions.

Notes and references

1 F. Hund, *Z. Phys.*, 1927, **43**, 805–826.
2 G. Gamow, *Nature*, 1928, **122**, 805–806.
3 D. Ley, D. Gerbig and P. R. Schreiner, *Org. Biomol. Chem.*, 2012, **10**, 3781–3790.
4 W. P. Huskey and R. L. Schowen, *J. Am. Chem. Soc.*, 1983, **105**, 5704–5706.
5 R. P. Bell, *The Tunnel Effect in Chemistry*, Chapman and Hall Ltd, London, 1980.
6 V. J. Shiner and M. L. Smith, *J. Am. Chem. Soc.*, 1961, **83**, 593–598.
7 R. P. Bell, *Trans. Faraday Soc.*, 1959, **55**, 1–4.
8 M. M. Kreevoy, D. Ostovic, D. G. Truhlar and B. C. Garrett, *J. Phys. Chem.*, 1986, **90**, 3766–3774.
9 W. H. Miller, *J. Am. Chem. Soc.*, 1979, **101**, 6810–6814.
10 S. Wierlacher, W. Sander and M. T. H. Liu, *J. Am. Chem. Soc.*, 1993, **115**, 8943–8953.
11 R. B. Woodward and H. Baer, *J. Am. Chem. Soc.*, 1944, **66**, 645–649.
12 P. R. Schreiner, H. P. Reisenauer, D. Ley, D. Gerbig, C.-H. Wu and W. D. Allen, *Science*, 2011, **332**, 1300–1303.
13 D. Ley, D. Gerbig, J. P. Wagner, H. P. Reisenauer and P. R. Schreiner, *J. Am. Chem. Soc.*, 2011, **133**, 13614–13621.
14 B. K. Carpenter, *Science*, 2011, **332**, 1269–1270.
15 B. K. Carpenter, *J. Am. Chem. Soc.*, 1983, **105**, 1700–1701.
16 H. Eyring, *J. Chem. Phys.*, 1935, **3**, 107–115.
17 M. G. Evans and M. Polanyi, *Trans. Faraday Soc.*, 1935, **31**, 875–894.
18 P. S. Zuev, R. S. Sheridan, T. V. Albu, D. G. Truhlar, D. A. Hrovat and W. T. Borden, *Science*, 2003, **299**, 867–870.
19 R. A. Moss, R. R. Sauers, R. S. Sheridan, J. Tian and P. S. Zuev, *J. Am. Chem. Soc.*, 2004, **126**, 10196–10197.
20 G. R. Shelton, D. A. Hrovat and W. T. Borden, *J. Am. Chem. Soc.*, 2006, **129**, 164–168.
21 A. Datta, D. A. Hrovat and W. T. Borden, *J. Am. Chem. Soc.*, 2008, **130**, 6684–6685.
22 R. A. Moss, G. J. Ho and W. Liu, *J. Am. Chem. Soc.*, 1992, **114**, 959–963.
23 R. A. Moss and M. E. Fantina, *J. Am. Chem. Soc.*, 1978, **100**, 6788–6790.
24 R. Bonneau, M. T. H. Liu and M. T. Rayez, *J. Am. Chem. Soc.*, 1989, **111**, 5973–5974.

25 G. J. Ho, K. Krogh-Jespersen, R. A. Moss, S. Shen, R. S. Sheridan and R. Subramanian, *J. Am. Chem. Soc.*, 1989, **111**, 6875–6877.
26 M. T. H. Liu and R. Bonneau, *J. Phys. Chem.*, 1989, **93**, 7298–7300.
27 H. P. Reisenauer, J. Romanski, G. Mloston and P. R. Schreiner, *Eur. J. Org. Chem.*, 2006, **2006**, 4813–4818.
28 P. R. Schreiner, H. P. Reisenauer, J. Romanski and G. Mloston, *Angew. Chem., Int. Ed.*, 2006, **45**, 3989–3992.
29 P. R. Schreiner and H. P. Reisenauer, *Angew. Chem., Int. Ed.*, 2008, **47**, 7071–7074.
30 P. Zuev and R. S. Sheridan, *J. Am. Chem. Soc.*, 1994, **116**, 4123–4124.
31 D. Gerbig, H. P. Reisenauer, C.-H. Wu, D. Ley, W. D. Allen and P. R. Schreiner, *J. Am. Chem. Soc.*, 2010, **132**, 7273–7275.
32 D. Gerbig, D. Ley, H. P. Reisenauer and P. R. Schreiner, *Beilstein J. Org. Chem.*, 2010, **6**, 1061–1069.
33 P. R. Schreiner, H. P. Reisenauer, F. C. Pickard IV, A. C. Simmonett, W. D. Allen, E. Mátyus and A. G. Császár, *Nature*, 2008, **453**, 906–909.
34 D. Gerbig, D. Ley and P. R. Schreiner, *Org. Lett.*, 2011, **13**, 3526–3529.
35 K. W. Egger and A. T. Cocks, *Helv. Chim. Acta*, 1973, **56**, 1516–1536.
36 J. Pacansky and J. S. Chang, *J. Chem. Phys.*, 1981, **74**, 5539–5546.
37 S. J. Blanksby and G. B. Ellison, *Acc. Chem. Res.*, 2003, **36**, 255–263.
38 The formation of **11** also provides firm experimental evidence for the generation of **9** as a decomposition product in the thermolysis of **13**.
39 J. P. Merrick, D. Moran and L. Radom, *J. Phys. Chem. A*, 2007, **111**, 11683–11700.
40 M. Razavy, *Quantum Theory of Tunneling*, World Scientific, Singapore, 2003.
41 A. Sen and A. Kohen, *J. Phys. Org. Chem.*, 2010, **23**, 613–619.
42 H.-H. Limbach, K. B. Schowen and R. L. Schowen, *J. Phys. Org. Chem.*, 2010, **23**, 586–605.
43 D. G. Truhlar, *J. Phys. Org. Chem.*, 2010, **23**, 660–676.
44 G. S. Hammond, *J. Am. Chem. Soc.*, 1955, **77**, 334–338.
45 A. Schellenberger and G. Oehme, *J. Prakt. Chem.*, 1964, **24**, 231–238.
46 CFOUR, Coupled-Cluster Techniques for Computational Chemistry, Quantum Chemical Program Package, http://www.cfour.de, (see ESI for full reference†).
47 J. Čížek, *J. Chem. Phys.*, 1966, **45**, 4256–4266.
48 K. Raghavachari, G. W. Trucks, J. A. Pople and M. Head-Gordon, *Chem. Phys. Lett.*, 1989, **157**, 479–483.
49 R. J. Bartlett, J. D. Watts, S. A. Kucharski and J. Noga, *Chem. Phys. Lett.*, 1990, **165**, 513–522.
50 J. F. Stanton, *Chem. Phys. Lett.*, 1997, **281**, 130–134.
51 J. T. H. Dunning, *J. Chem. Phys.*, 1989, **90**, 1007–1023.
52 F. Wennmohs and F. Neese, *Chem. Phys.*, 2008, **343**, 217–230.
53 F. Neese, A. Hansen, F. Wennmohs and S. Grimme, *Acc. Chem. Res.*, 2009, **42**, 641–648.
54 F. Neese, *Wiley Interdiscip. Rev.: Comput. Mol. Sci.*, 2012, **2**, 73–78.
55 Y. Zhao and D. Truhlar, *Theor. Chem. Acc.*, 2008, **120**, 215–241.
56 Y. Zhao and D. G. Truhlar, *Acc. Chem. Res.*, 2008, **41**, 157–167.
57 H. P. Hratchian and H. B. Schlegel, *J. Chem. Phys.*, 2004, **120**, 9918–9924.
58 *Gaussian09, Revision B.02*, Gaussian, Inc., Wallingford CT, 2009, (see ESI for full reference†).
59 Mathematica, *Version 7.0.1*, Wolfram Research Inc., Champaign IL, 2008.

